XMM-Newton SPECTROSCOPY OF TWO HYADES STARS

E. Franciosini J. Sanz-Forcada, A. Maggio, R. Pallavicini [a],

[a]INAF - Osservatorio Astronomico di Palermo, Piazza del Parlamento 1, I-90134 Palermo, Italy

We present the results of XMM-Newton observations of two Hyades stars: the giant θ^1 Tau and the solar-type star VB 50. From the analysis of RGS and EPIC spectra we derive the temperature structure and chemical abundances of the coronae of the two stars.

1. Introduction

The study of stars in open clusters is a valuable tool for our understanding of stellar coronae, since it allows us to compare stars having the same age and chemical composition but different masses and evolutionary states.

The Hyades open cluster (age $\sim$ 600 Myr) is one of the best studied open clusters thanks to its proximity. It has been observed in X-rays with *Einstein* [1,2] and *ROSAT* [3–5]. The cluster contains four giants that have all been detected in X-rays, although with very different X-ray luminosities.

We have selected as targets for our *XMM-Newton* observations the X-ray brightest of the four Hyades giants, θ^1 Tau = VB 71 (spectral type K0 III, d = 48.40 pc [6]), with an X-ray luminosity $L_X \sim 1 \times 10^{30}$ erg sec^{-1}, and one of the X-ray brightest solar-type main-sequence stars, VB 71 (spectral type G1 V, d = 44.94 pc [6]), which has $L_X \sim 6 \times 10^{29}$ erg sec^{-1}.

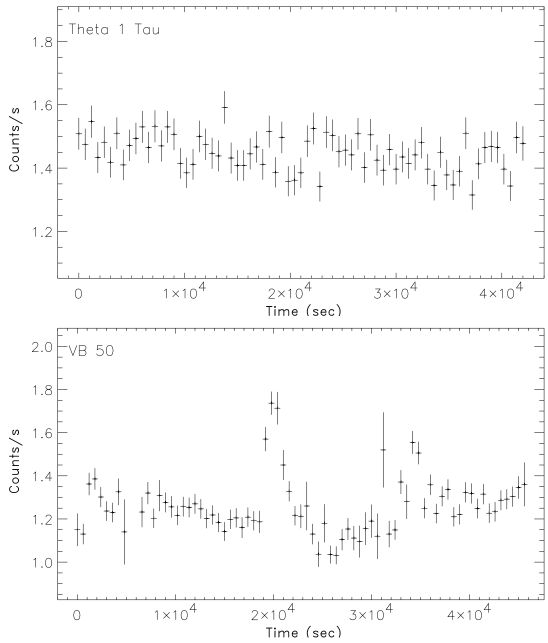

Figure 1. EPIC PN light curve of θ^1 Tau = VB 71 (*top*) and VB 50 (*bottom*). Data are binned over 600 sec. Note the higher variability of VB 50

2. Observations and data analysis

θ^1 Tau was observed on September 3, 2000 for 48 ksec (ID 0101440501). The thick filter was used for both MOS and PN. Effective exposure times are 48 ksec for RGS, 40 ksec for MOS and 42.5 ksec for PN.

VB 50 was observed on September 9, 2000 (ID 0101440601) for 50 ksec and again on March 5–6, 2002 (ID 0101441501) for 58 ksec. For the first observation only EPIC data are available; here we present the results for the second one. The medium filter was used for both MOS and PN. Effective exposure times are 57.5 ksec for RGS, 48 ksec for MOS and 46.5 ksec for PN.

Data analysis was performed using standard tasks in SAS v.5.3.3. EPIC source and background spectra have been extracted using an extraction region of 1′ radius. For spectral fitting, both EPIC and RGS spectra have been binned in order to have at least 30 counts per energy bin. Spectral fitting has been performed in XSPEC v.11.2.0.

Fig. 1 shows the PN light curves of the two stars. The X-ray emission of θ^1 Tau is steady, showing only low-level fluctuations around a mean count rate of $\sim$ 1.5 counts/sec in the PN instrument, and $\sim$ 0.5 counts/sec in each MOS instrument. On the contrary, VB 50 appears to be more active, showing higher variability and a few small flares.

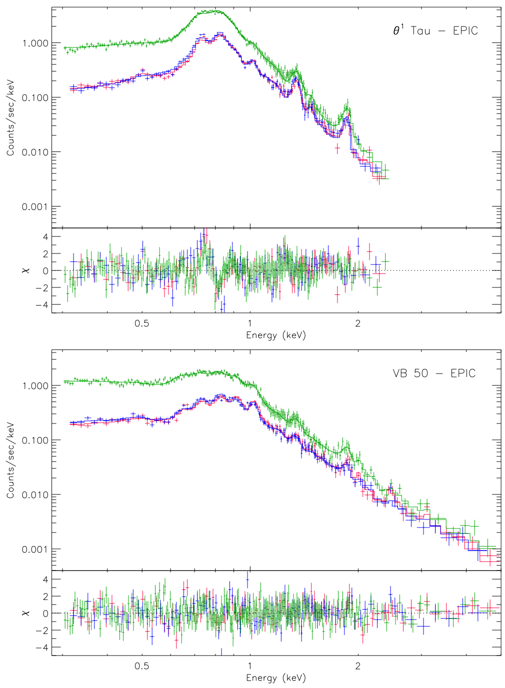

Figure 2. EPIC MOS1 (*blue*), MOS2 (*red*) and PN (*green*) spectra of θ^1 Tau and VB 50. The individual best-fit 2-T models are also shown. The spectrum of θ^1 Tau is background dominated for $E > 2.5$ keV

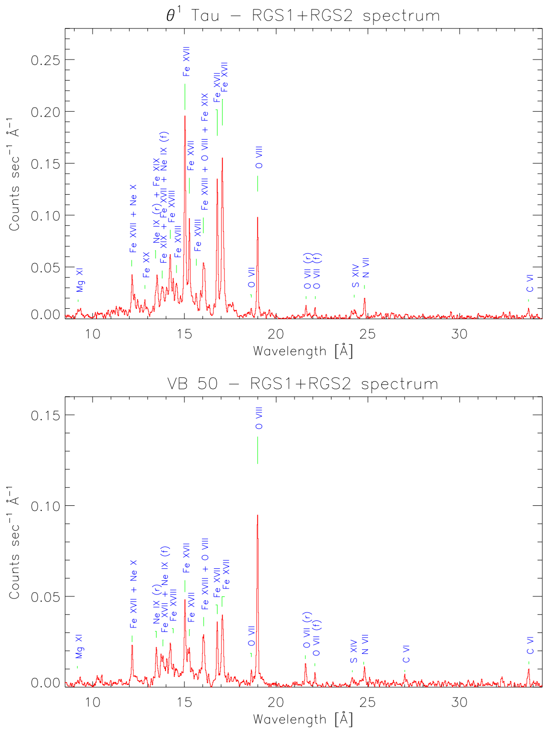

Figure 3. RGS1+RGS2 combined spectrum of θ^1 Tau and VB 50. The most prominent lines are indicated

3. Spectral analysis

We have fitted separately the RGS1+RGS2, MOS1, MOS2 and PN spectra using two-temperature thermal models and adopting the APEC v.1.2.0 emissivities. The abundances of C, N, O, Ne, Mg, Si, S, Fe, and Ni were treated as individual free parameters. The interstellar hydrogen column density, which was not constrained by the fit, was fixed to $N_H = 10^{19}$ cm^{-3}, as expected for the distance of the Hyades. EPIC spectra have been fitted at energies above 0.3 keV, while RGS spectra were fitted in the 5–35 Å wavelength band. The best-fit parameters are given in Table 1. The EPIC spectra together with the best-fit models are shown in Fig. 2.

Some of the fits are not acceptable, from a statistical point of view, due to large residuals expecially in the ranges 0.6–0.9 keV. Adding a third plasma component does not improve the fit: indeed, any additional component always converges to one of the first two. The large residuals may arise from inadequacies of the currently available plasma codes or from calibration problems.

We also note that, while in general the best-fit parameters derived from different instruments agree within the errors, some discrepancies are still present (marked in boldface in Table 1), that are most likely due to uncertainties in the cross-calibration of the instruments. Note in particular the higher abundance of Fe and Ne derived from the PN spectrum of θ^1 Tau.

We find that the corona of VB 50 is hotter than that of θ^1 Tau. θ^1 Tau has temperatures of $\sim$ 4 and $\sim$ 7 MK, with emission measures of $\sim 4-8 \times 10^{52}$ cm^{-3} and $\sim 4 \times 10^{52}$ cm^{-3}, respectively; VB 50 has a very similar low temperature component, while the hotter component has $T \sim 18$ MK and $EM \sim 1.4 \times 10^{52}$ cm^{-3}.

Fig. 3 shows the co-added RGS1 and RGS2 spectra of θ^1 Tau and VB 50. The X-ray spectrum of θ^1 Tau is largely dominated by the bright Fe XVII and Fe XVIII L-shell lines, indicating a dominant temperature component around 0.6 keV, confirmed by our analysis (Table 1). However, other emission lines are observed, e.g.

Table 1
Best-fit parameters for θ^1 Tau and VB 50. Errors are 90% confidence ranges computed for one interesting parameter. Discrepant values are marked in boldface

	θ^1 **Tau**				**VB 50**			
	RGS1+RGS2	MOS1	MOS2	PN	RGS1+RGS2	MOS1	MOS2	PN
kT_1^a	$0.25^{+0.02}_{-0.02}$	$0.36^{+0.11}_{-0.04}$	$0.34^{+0.02}_{-0.01}$	$0.26^{+0.01}_{-0.01}$	$\mathbf{0.27^{+0.03}_{-0.02}}$	$0.38^{+0.02}_{-0.02}$	$0.42^{+0.01}_{-0.01}$	$0.38^{+0.02}_{-0.02}$
kT_2^a	$0.57^{+0.01}_{-0.01}$	$0.59^{+0.07}_{-0.02}$	$0.59^{+0.04}_{-0.02}$	$0.57^{+0.01}_{-0.01}$	$\mathbf{0.65^{+0.03}_{-0.02}}$	$1.48^{+0.11}_{-0.10}$	$1.65^{+0.17}_{-0.12}$	$1.58^{+0.13}_{-0.11}$
EM_1^b	$3.4^{+1.1}_{-1.0}$	$5.8^{+2.2}_{-2.1}$	$7.8^{+1.2}_{-1.7}$	$3.7^{+0.8}_{-0.9}$	$\mathbf{1.9^{+0.6}_{-0.6}}$	$4.0^{+0.8}_{-0.9}$	$5.7^{+0.2}_{-0.2}$	$5.0^{+0.8}_{-0.9}$
EM_2^b	$4.6^{+0.7}_{-0.7}$	$4.7^{+1.5}_{-2.3}$	$3.8^{+0.6}_{-1.3}$	$3.5^{+0.5}_{-0.5}$	$\mathbf{3.1^{+0.5}_{-0.4}}$	$1.5^{+0.2}_{-0.2}$	$1.4^{+0.1}_{-0.1}$	$1.3^{+0.2}_{-0.2}$
C	$0.14^{+0.09}_{-0.09}$	$0.20^{+1.92}_{-0.20}$	$0.00^{+0.94}_{-\dots}$	$0.00^{+0.18}_{-\dots}$	$0.23^{+0.18}_{-0.16}$	$0.18^{+1.30}_{-0.18}$	$0.59^{+1.23}_{-0.59}$	$0.00^{+0.32}_{-\dots}$
N	$0.37^{+0.19}_{-0.14}$	$0.52^{+1.16}_{-0.48}$	$0.00^{+0.18}_{-\dots}$	$0.74^{+0.46}_{-0.32}$	$0.38^{+0.20}_{-0.16}$	$0.00^{+0.41}_{-\dots}$	$0.00^{+0.35}_{-\dots}$	$0.47^{+0.44}_{-0.29}$
O	$0.12^{+0.04}_{-0.03}$	$0.07^{+0.09}_{-0.04}$	$0.10^{+0.04}_{-0.03}$	$0.19^{+0.06}_{-0.04}$	$0.21^{+0.05}_{-0.04}$	$0.19^{+0.09}_{-0.05}$	$0.15^{+0.07}_{-0.05}$	$0.21^{+0.07}_{-0.04}$
Ne	$0.23^{+0.08}_{-0.08}$	$0.22^{+0.11}_{-0.07}$	$0.22^{+0.07}_{-0.06}$	$\mathbf{0.58^{+0.16}_{-0.13}}$	$0.67^{+0.16}_{-0.13}$	$0.91^{+0.30}_{-0.17}$	$0.58^{+0.17}_{-0.13}$	$0.79^{+0.21}_{-0.12}$
Mg	$0.80^{+0.25}_{-0.22}$	$0.58^{+0.26}_{-0.12}$	$0.73^{+0.20}_{-0.09}$	$1.00^{+0.22}_{-0.16}$	$0.34^{+0.20}_{-0.19}$	$0.45^{+0.20}_{-0.15}$	$0.21^{+0.11}_{-0.08}$	$0.44^{+0.17}_{-0.10}$
Si	$0.26^{+0.51}_{-0.26}$	$0.42^{+0.19}_{-0.11}$	$0.57^{+0.19}_{-0.10}$	$0.64^{+0.17}_{-0.14}$	$0.30^{+0.41}_{-0.30}$	$0.63^{+0.27}_{-0.20}$	$0.38^{+0.16}_{-0.13}$	$0.60^{+0.22}_{-0.16}$
S	$0.08^{+0.22}_{-0.08}$	$0.00^{+0.62}_{-\dots}$	$0.00^{+0.29}_{-\dots}$	$0.00^{+0.22}_{-\dots}$	$0.00^{+0.20}_{-\dots}$	$0.72^{+0.45}_{-0.35}$	$0.21^{+0.36}_{-0.21}$	$0.32^{+0.39}_{-0.26}$
Fe	$0.62^{+0.10}_{-0.09}$	$0.48^{+0.20}_{-0.08}$	$0.53^{+0.13}_{-0.02}$	$\mathbf{0.92^{+0.17}_{-0.11}}$	$0.25^{+0.04}_{-0.03}$	$0.30^{+0.10}_{-0.06}$	$0.20^{+0.06}_{-0.05}$	$0.26^{+0.07}_{-0.05}$
Ni	$0.00^{+0.10}_{-\dots}$	$0.00^{+0.14}_{-\dots}$	$0.00^{+0.09}_{-\dots}$	$0.00^{+0.28}_{-\dots}$	$\mathbf{0.00^{+0.15}_{-\dots}}$	$2.77^{+1.19}_{-0.86}$	$1.59^{+0.71}_{-0.55}$	$2.48^{+1.05}_{-0.71}$
χ^2_r/dof	2.60/328	2.05/85	2.66/83	1.23/250	2.23/206	1.40/103	1.72/96	1.12/267
$F^c_{0.1-2.4}$	3.92	3.85	4.12	3.96	2.26	2.36	2.48	2.56

[a] kT in keV
[b] EM in units of 10^{52} cm^{-3}
[c] Unabsorbed flux in the 0.1 – 2.4 keV bands, in units of 10^{-12} erg cm^{-2} sec^{-1}

Lyα transitions from O VIII, Ne X, N VII, and C VI.

In VB 50 the same lines are present but the Fe line/continuum ratio is lower, due to the lower metallicity of VB 50.

4. Emission measure distribution

We have derived the Emission Measure distribution vs. temperature, $EM(T)$, using a line-based method. Flux measurements were made using the tools provided by the PINTofALE package [7]. We started with a trial $EM(T)$ in order to predict the line fluxes, which were then compared to the observed ones. An iterative process was then followed in order to improve the fit of the observed line fluxes.

Elemental abundances are also evaluated during the fitting process of the EM distribution. The fit was first made with Fe lines only, and the other elements were progressively added one by one. This method permits to extend the temperature coverage of $EM(T)$ while the abundances are being determined.

The EM distributions obtained for the two sources have similar shapes, but VB 50 contains hotter material than θ^1 Tau (Fig. 4), in agreement with the results of the 2-T fits.

5. Abundances

We find that in general the abundances derived from the EM distribution are consistent with those obtained from the 2-T fitting, with the exception of Ni in θ^1 Tau and S in VB 50, for which higher values are derived from $EM(T)$. In Fig. 5 we show the abundances derived from the 2-T fits for the different instruments, ordered by increasing First Ionization Potential (FIP). θ^1 Tau shows some indication of a solar-like FIP effect, with higher abundances of Mg and Fe (low-FIP) with respect to O and Ne (high-FIP). On the contrary, the abundances of VB 50 are all at about the same level, except for Ne which is relatively overabundant.

The 2-T fits of RGS spectra hint to a higher N/C ratio for θ^1 Tau with respect to VB 50. For a cosmic abundance plasma in collisional equilibrium, the ratio R_{NC} of the N VII and C VI line fluxes is almost independent of temperature and is expected to be ≤ 0.57 (see [8]). These authors suggested that the enhancement of this ratio observed in a sample of giants might be due to the exposure of CNO-cycle processed material at the surfaces of evolved stars. From our measured line fluxes we derive $R_{NC} = 0.55 \pm 0.23$ for VB 50

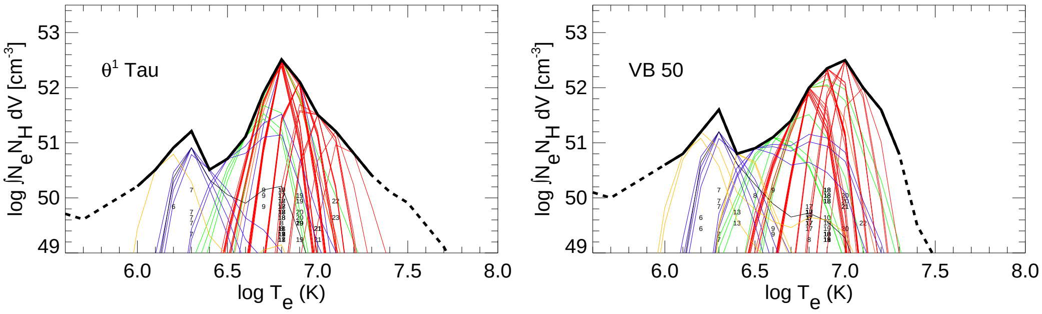

Figure 4. Reconstructed EM distribution vs. temperature of θ^1 Tau and VB 50

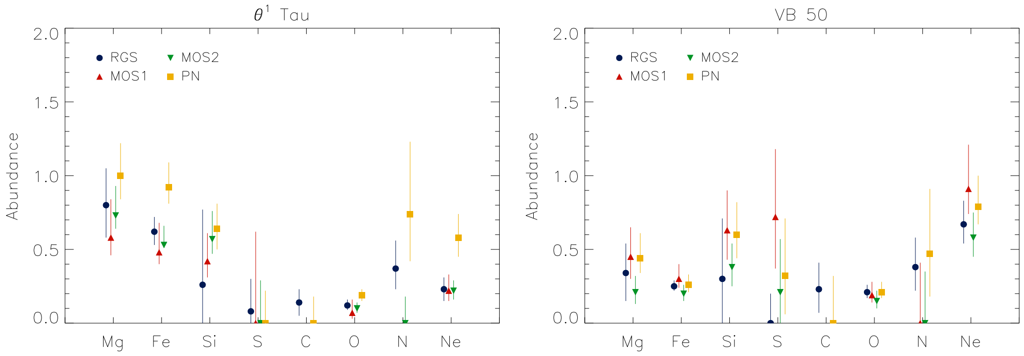

Figure 5. Elemental abundances derived from the 2-T fit, ordered by increasing FIP. Poorly constrained values have been excluded from the figure for the sake of clarity

and $R_{NC} = 1.21 \pm 0.64$ for θ^1 Tau. Our result is therefore marginally consistent with the conclusions by [8].

The low S/N of the RGS spectra at the O VII triplet in both stars prevents an accurate determination of the fluxes of the intercombination and forbidden lines; however their ratio is consistent with the low-density limit.

6. Conclusions

- The corona of VB 50 is hotter than that of θ^1 Tau, reaching temperatures a factor of ~ 2 higher.
- A solar-like FIP effect is present in VB 71 while a possible inverse FIP effect may be present in VB 50.
- Apparently the metallicity of θ^1 Tau is about twice that of VB 50, and both are significantly lower than the photospheric metallicity of Hyades stars ([Fe/H] $= +0.13 \pm 0.02$ [9]).
- Some discrepancies exist between the abundances derived from different instruments which point at possible uncertainties in their cross-calibration.

REFERENCES

1. Stern, R. A., Zolcinski, M.-C., Antiochos, S. K., & Underwood, J. H. 1981, ApJ, 249, 647
2. Micela, G., Sciortino, S., Vaiana, G. S., *et al.* 1988, ApJ, 325, 798
3. Stern, R. A., Schmitt, J. H. M. M., Pye, J. P., *et al.* 1994, ApJ, 427, 808
4. Pye, J. P., Hodgkin, S. T., Stern, R. A., & Stauffer, J. R. 1994, MNRAS, 266, 798
5. Stern, R. A., Schmitt, J. H. M. M., & Kahabka, P. T. 1995, ApJ, 448, 683
6. ESA 1997, The Hipparcos and Tycho catalogues, ESA SP-1200
7. Kashyap, V. & Drake, J. J. 2000, BASI, 28, 475
8. Schmitt, J. H. M. M. & Ness, J.-U. 2002, A&A, 388, L13
9. Friel, E. D. & Boesgaard, A. M. 1992, ApJ, 387, 170